



OPEN

# Organized Disassembly of Photosynthesis During Programmed Cell Death Mediated By Long Chain Bases

Alonso Zavafer<sup>1</sup>, Ariadna González-Solís<sup>2</sup>, Silvia Palacios-Bahena<sup>2</sup>, Mariana Saucedo-García<sup>3</sup>, Cinthya Tapia de Aquino<sup>2</sup>, Sonia Vázquez-Santana<sup>4</sup>, Beatriz King-Díaz<sup>2</sup> & Marina Gavilanes-Ruiz<sup>2</sup>✉

In plants, pathogen triggered programmed cell death (PCD) is frequently mediated by polar lipid molecules referred as long chain bases (LCBs) or ceramides. PCD interceded by LCBs is a well-organized process where several cell organelles play important roles. In fact, light-dependent reactions in the chloroplast have been proposed as major players during PCD, however, the functional aspects of the chloroplast during PCD are largely unknown. For this reason, we investigated events that lead to disassembly of the chloroplast during PCD mediated by LCBs. To do so, LCB elevation was induced with *Pseudomonas syringae* pv. *tomato* (a non-host pathogen) or Fumonisin B1 in *Phaseolus vulgaris*. Then, we performed biochemical tests to detect PCD triggering events (phytosphingosine rises, MPK activation and H<sub>2</sub>O<sub>2</sub> generation) followed by chloroplast structural and functional tests. Observations of the chloroplast, via optical phenotyping methods combined with microscopy, indicated that the loss of photosynthetic linear electron transport coincides with the organized ultrastructure disassembly. In addition, structural changes occurred in parallel with accumulation of H<sub>2</sub>O<sub>2</sub> inside the chloroplast. These features revealed the collapse of chloroplast integrity and function as a mechanism leading to the irreversible execution of the PCD promoted by LCBs.

The simplest plant sphingolipids are long chain bases (LCBs), which have a signaling role during stomata closure, cold response and programmed cell death or PCD (immunity associated)<sup>1–9</sup>. In the case of PCD associated with pathogen immunity, there has been indication of a transient rise of long chain bases (LCBs): sphinganine<sup>10,11</sup> and phytosphingosine<sup>12</sup>. Plants express PCD during differentiation, development, senescence, and immunity, but it is the latter in which LCBs have been demonstrated as transducers. The Hypersensitive Response (HR) is a PCD form which is a common and powerful mechanism of plant defense against pathogens<sup>13,14</sup>. HR is visualized as a dry tissue spot developed at the entry site of certain pathogens, wherein cells launch a death program. This prevents the supply of nutrients to the biotroph intruder, avoiding its dissemination<sup>15</sup>. LCBs have been suggested as second messengers in the HR-PCD involved in forms of plant immunity. Interestingly, some other signaling events in this PCD transduction pathway have also been described: generation of reactive oxygen species generation (ROS)<sup>11–18</sup>, MPK6 activation<sup>11</sup> and a calcium surge<sup>10</sup>, but their integration as a whole chain of events remains to be established.

Some studies on PCD related to immunity have shown effects on the chloroplast: (1) PCD evoked by *Pseudomonas syringae* through MPK6 intermediation results in an inhibition of CO<sub>2</sub> fixation and H<sub>2</sub>O<sub>2</sub> accumulation in chloroplasts<sup>19</sup>; (2) PCD elicited by inhibition of the electron transport beyond Q<sub>A</sub> in photosystem II is related to systemic immunity<sup>20</sup>; (3) PCD produced by an avirulent strain of *Pseudomonas syringae* was suggested to be influenced by disassembly of the photosynthetic complexes, probably due to ROS generation in the

<sup>1</sup>Climate Change Cluster, University of Technology Sydney, Faculty of Science Building 4, Level 6 Corner of Thomas and, Harris St, Ultimo NSW 2007, Sydney, Australia. <sup>2</sup>Dpto. de Bioquímica, Facultad de Química, Conjunto E. Universidad Nacional Autónoma de México (UNAM). Ciudad Universitaria, 04510, Ciudad de México, México.

<sup>3</sup>Instituto de Ciencias Agropecuarias, Universidad Autónoma del Estado de Hidalgo, Tulancingo, Hidalgo, México.

<sup>4</sup>Dpto. de Biología Comparada, Facultad de Ciencias, Universidad Nacional Autónoma de México (UNAM). Ciudad Universitaria, 04510, Ciudad de México, México. ✉e-mail: [gavilan@unam.mx](mailto:gavilan@unam.mx)

chloroplast<sup>21</sup>. Moreover, it has been recognized that photosynthetic activity is interrupted upon pathogen infection<sup>22–24</sup>. All this diverse information suggests that the chloroplast and its photosynthetic activity are involved in the PCD process.

In parallel, evidences dealing with the PCD-HR mediated by LCBs suggest an association with the chloroplast: (1) PCD elicited by fumonisin B1 (FB1, a mycotoxin that evokes LCB accumulation<sup>25</sup>) is light-dependent<sup>16</sup>; (2) PCD induced by FB1 and mediated by MPK6<sup>11</sup> promotes extensive chloroplast damage and induces H<sub>2</sub>O<sub>2</sub> formation inside the chloroplasts<sup>11,19</sup>. However, a study of the chloroplast and its function during HR-PCD that is mediated by LCBs has not been specifically addressed.

Therefore, these and other unknown events dealing with the chloroplast need to be identified and positioned in a single sequence in order to establish a clear functional context. For this reason, we have induced PCD in *Phaseolus vulgaris* using two LCB eliciting treatments: FB1 and a non-host pathogen that induces HR-PCD. Then, we explored if LCB accumulation took place in both treatments and measured some biochemical responses such as reactive oxygen species formation and MAP kinases activation. Then, we analyzed the chloroplast ultrastructure and the functioning of its light-dependent reactions. Here, we provide direct evidence that there is a direct organized and irreversible collapse of the chloroplast that leads to the PCD mediated by LCBs.

## Materials and methods

**Chemicals.** Fumonisin B1, sphinganine, phytosphingosine, myelin basic protein (MBP),  $\alpha$ -casein bovine milk, and calf-thymus histone III were purchased from Sigma Chemicals (St. Louis Mo). D-erythro C20-sphingosine was purchased from Matreya Inc. (Pleasant Gap, PA). Silwet L-77 was obtained from Chemtura Corporation S. de R.L. de C.V. (Mexico City, México).  $\gamma$ -[<sup>32</sup>P]-ATP (Easy Tides 3000 Ci/mmol-10 mCi/ml, pH 7.6 was purchased from PerkinElmer (Austin, Tx).

**Biological material.** *Phaseolus vulgaris* var. Canario (common bean) plants were grown in agrolite, watered with Hoagland solution and maintained under a natural photoperiod at 28 °C in a greenhouse. *Pseudomonas syringae* pv. *tomato* DC3000 avrRPM1 (Pst), a strain that elicits a defense response in *Phaseolus*, was cultured in solid B King medium with rifampicin and tetracycline at 50  $\mu$ g/ml. Fresh cultures were resuspended in 10 mM MgCl<sub>2</sub> and then leaf-infiltrated.

**In planta treatments.** MgCl<sub>2</sub>, Silwet L-77, FB1, sphinganine (SN), salicylic acid (SA) and *Pseudomonas syringae* were infiltrated in fully expanded leaves attached to healthy 4–6-week-old *Phaseolus* plants. Infiltration was done on the leaf abaxial surface in 4–6 points per leaf with a needleless syringe<sup>26</sup>. Every point was infiltrated with 20  $\mu$ L of the following compounds: 10 mM MgCl<sub>2</sub> (as control), 0.05% Silwet L-77 (as control), 5–50  $\mu$ M FB1 dissolved in 10 mM MgCl<sub>2</sub>, 40  $\mu$ M SN dissolved in 0.05% Silwet L-77, 1 mM salicylic acid (SA), pH 7 and a suspension of *Pseudomonas syringae* pv. *tomato* at  $1 \times 10^5$  to  $1 \times 10^8$  CFU (colony forming units) per ml as indicated.

Samples at the infiltration sites were taken in the interval from 0 to 48 h after treatments as indicated. Treatments with MgCl<sub>2</sub>, Silwet L-77, FB1, Pst, SN or SA were performed while the leaves were attached to the plant and then all measurements were carried out. A photographic record of the evolution of leaves upon different treatments was followed.

**Electrolyte leakage assay.** Leaf disks of 1.0 cm diameter containing the infiltration points were cut at every infiltration time, weighed and electrolyte leakage was determined with a conductimeter Conmet1, Hanna Instruments (Woonsocket, RI)<sup>27</sup>. Briefly, leaf disks were submerged in double distilled water under moderate stirring and medium conductance was measured at several times. Electrolyte leakage was expressed following the formula  $ES = EC1/EC2 \times 100$ , where ES corresponds to final conductivity of the sample, E1 corresponds to the electrical conductivity measured at 24, 48 and 72 h and EC2 corresponds to the conductivity measured at the end of the experiment when leaf disks were boiled to release total electrolytes into the medium.

**Determination of MAPK activity.** *Phaseolus* leaves were infiltrated with MgCl<sub>2</sub>, Silwet L-77, FB1, SN, SA or *Pseudomonas syringae* pv. *tomato* during the indicated times and immediately frozen and maintained at –70 °C. Then, at periods no longer than one week, leaves were homogenized to obtain the soluble fractions and in-gel MAPK activity was performed supplementing MBP to the polyacrylamide matrix to serve as phosphorylation substrate using  $\gamma$ -[<sup>32</sup>P]-ATP. This assay was performed using  $\alpha$ -casein and type III histone as negative controls to identify specific MAPK phosphorylating activity.

**Determination of H<sub>2</sub>O<sub>2</sub> in situ.** Leaf disks of 1.0 cm diameter containing the infiltration treatments were immediately submerged in a solution of 3,3-diaminobenzidine (DAB)<sup>28</sup>. The H<sub>2</sub>O<sub>2</sub> in the leaf tissue was visualized by a brown-reddish precipitate. Images were photographed (Moticam 2300, 3.0 M Pixel USB 2.0) coupled to a dissection microscope using the software Motic Images Plus 2.0 ml (Motic China Group [www.motic.com](http://www.motic.com)).

**Determination of H<sub>2</sub>O<sub>2</sub> in solution.** Total levels of H<sub>2</sub>O<sub>2</sub> were determined in the infiltrated tissue. Briefly, leaf disks of 1.0 cm diameter were sectioned from the leaf sites infiltrated with MgCl<sub>2</sub>, FB1 or Pst and immediately homogenized and centrifuged. Aliquots from the supernatant were rapidly withdrawn to determine the ferric-xylenol orange complex<sup>29</sup>.

**Determination of LCBs.** Extraction of LCBs was done according to Markham *et al.*<sup>30</sup>, starting from a microsomal fraction equivalent to 1.0 mg of fresh weight tissue. Briefly, the membrane fraction was supplemented with 2 nmol of D-erythro sphingosine as internal standard, 1 ml dioxane, 1.0 ml of 10% Ba(OH)<sub>2</sub>, and incubated at 110 °C during 16 h. Then 2 ml of 2% ammonium sulphate and 2 ml of diethyl ether were added. The organic phase was evaporated under a nitrogen flow until dry and the residue used for LCB determination. This was done by

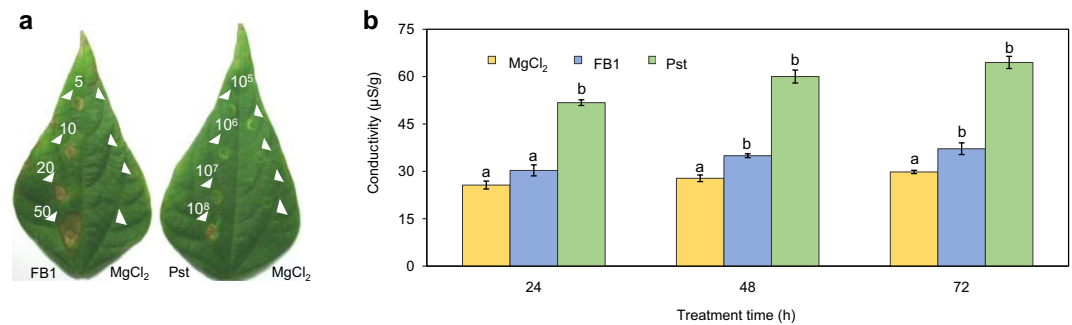


**Figure 1.** FB1 and Pst produce common PCD-HR macroscopic responses in *Phaseolus* leaves. **(a)** PCD-HR lesions. Leaves were infiltrated *in planta* with different concentrations of FB1 and Pst. Leaf at left shows points of infiltration with 1, 5, 10 and 20  $\mu\text{M}$  FB1 as indicated. Leaf at right shows points of infiltration with  $1 \times 10^5$ ,  $1 \times 10^6$ ,  $1 \times 10^7$ ,  $1 \times 10^8$  CFU/ml Pst as indicated. Arrows at the right side of both leaves show the infiltration of 10 mM  $\text{MgCl}_2$ . Image shows lesions recorded after seven days of infiltration. Experiments were  $n > 8$  technical repeats from at least three biological replicates. **(b)** Electrolyte leakage. *Phaseolus* leaves were infiltrated *in planta* with 10  $\mu\text{M}$  FB1 or  $1 \times 10^8$  UFC/ml Pst at the indicated times and infiltrated areas were cut, weighed and subjected to solute leakiness determination. Average values of  $n > 8$  technical repeats from three biological replicates  $\pm$  standard error (s.e.m.). A mean comparison using a one-way ANOVA was done with a Tukey post-hoc test with  $p < 0.05$ .  $\text{MgCl}_2$  was used as reference for comparison at each time point. <sup>a</sup>No statistical difference between the control groups ( $\text{MgCl}_2$ ). <sup>b</sup>Statistical differences between  $\text{MgCl}_2$  and FB1 or Pst treatments.

LCB derivatization with NDA (naphtalen-2,3-dicarboxy dialdehyde)<sup>31</sup>. Once derivatized, the samples were analyzed with a Shimadzu HPLC system with an UV detector (Mod. SPD-10AV).

**Protein determination.** This was done according to Bradford (Bio-Rad, <http://www.bio-rad.com/>) using the Bio Rad Kit according to the manufacturer instructions.

**Determination of chlorophyll *a* fluorescence.** This was performed *in planta* at the infiltration sites as follows: The leaf areas exposed to the treatments at the indicated times were dark-adapted for 10 min and then illuminated with continuous light (650 nm peak wavelength,  $2800 \mu\text{mol photon m}^{-2} \text{s}^{-1}$ ). Chlorophyll *a* fluorescence was recorded during 1 s. The measurements were taken at infiltration times of 0, 8, 12, 24 and 48 h. Fast rise of the chlorophyll *a* fluorescence was measured with a Multifunctional Plant Efficiency Analyzer (M-PEA) (Hansatech Instruments Ltd., Norfolk, England).

**Determination of P700/P700<sup>+</sup>.** Simultaneously with the measurements of chlorophyll *a* fluorescence, plastocyanin (PC), P700 and ferredoxin reduction/oxidation were measured using the 820 nm transmission change (far red light 820 nm peak wavelength) with MPEA (Hansatech Instruments Ltd., Norfolk, England).

**Determination of chloroplast ultrastructure.** Leaf disks of 0.5 cm diameter were cut from the leaves infiltrated with  $\text{MgCl}_2$  (as control), FB1 solution or *Pseudomonas syringae* pv. *tomato* suspension. After the indicated times, the leaf disks were fixed in 100 mM phosphate buffer (pH 7.2) and 3% glutaraldehyde (v:v) at 4 °C, dehydrated and embedded in epon:polypropylene oxide. Sections of 80 nm were contrasted with uranyl acetate and lead citrate. Samples were observed with a Jeol 1200 EXII electron microscope (Jeol Ltd., <http://www.jeol.com/>) operated at 60 kV. Images were processed with Photoshop imaging software, version 8.0.1 (Adobe Systems, <http://www.adobe.com/products/photoshop/family/>).

**Determination of chloroplast autofluorescence.** Infiltrated leaf disks were fixed as for the ultrastructural analysis, but thin sections from the disks were observed in a confocal microscope Olympus FV1000 using a wavelength excitation of 635 nm and a wavelength emission of 664 nm for chloroplast autofluorescence.

**Statistical analysis.** All the results shown were the average values obtained from at least three independently grown/processed lots of plants. Statistical analyses were processed using Microsoft Excel 2007, SPSS 17 and Origin 7.0 as detailed in every experiment. All images were processed using ImageJ 1.2<sup>32</sup>.

## Results

### FB1 and *Pseudomonas syringae* pv. *tomato* induce similar responses associated to a PCD-HR in *Phaseolus vulgaris*.

In order to confirm that *Phaseolus* was FB1-sensitive as it occurs in many, but not all species<sup>33,34</sup>, leaves were infiltrated with 5 to 50  $\mu\text{M}$  FB1 (Fig. 1a). It was observed that the toxin produced a delimited spot the size of which was concentration-dependent (Fig. 1a, left leaf) and started to be visible 24–48 h after 10  $\mu\text{M}$  FB1 infiltration. Since non-host species can produce a hypersensitive response (HR) as part of a defense reaction, we infiltrated  $10^5$ – $10^8$  CFU/ml of a suspension from *Pseudomonas syringae* pv. *tomato* (Pst), a non-host pathogen, to bean leaves. Figure 1a (right leaf) shows that Pst suspension developed a necrotic zone the size of which was pathogen concentration-dependent and that was visible at 18–24 h after infiltration. Dead tissue remained circumscribed to the site of inoculation with FB1 or Pst, as it occurs in the classical HR and not

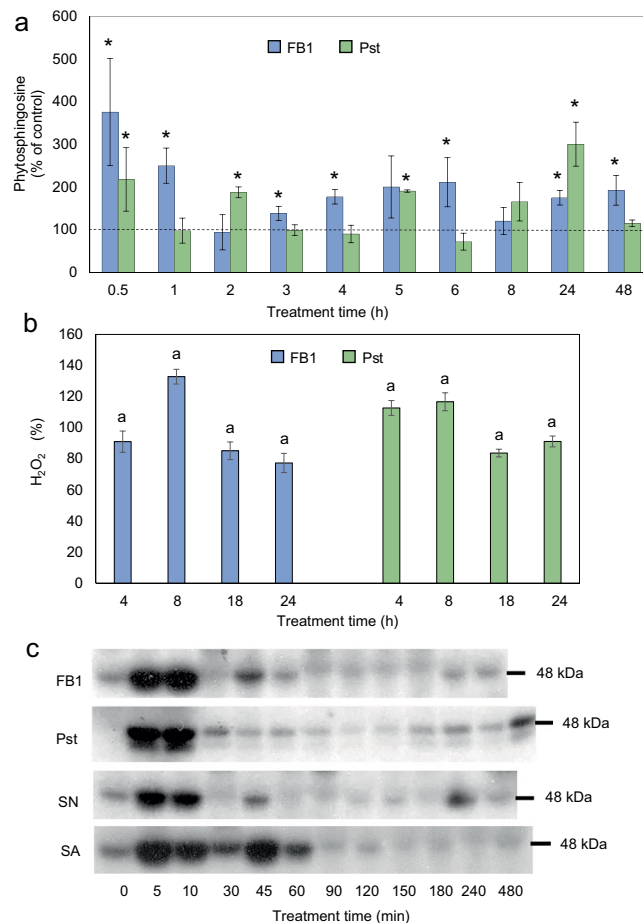


**Figure 2.** Pst and FB1 produce molecular responses associated to the PCD-HR mediated by LCB accumulation. **(a)** Long chain base levels. *Phaseolus* leaves were infiltrated *in planta* with 10  $\mu$ M FB1 or  $1 \times 10^8$  CFU/ml Pst and at the indicated times, infiltrated leaf sections were used to isolate microsomal fractions to quantitate phytosphingosine levels. MgCl<sub>2</sub>-infiltrated leaves were used as controls and processed exactly in the same way that the FB1- or Pst-infiltrated leaves. The results are expressed in terms of the phytosphingosine levels as compared to the respective MgCl<sub>2</sub>-infiltrated sample (100%), processed at every time. Average values of  $n > 6$  technical repeats from three biological replicates  $\pm$  standard error (s.e.m.). A mean comparison using a one-way ANOVA was done with a Tukey mean difference plot post-hoc test with  $p < 0.05$ . Leaves infiltrated with MgCl<sub>2</sub> were used as reference for comparison at each time point. **(b)** H<sub>2</sub>O<sub>2</sub> levels. *Phaseolus* leaves were infiltrated *in planta* with 10 mM MgCl<sub>2</sub>, 50  $\mu$ M FB1 or  $1 \times 10^8$  CFU/ml Pst and at the indicated times the infiltrated tissue was processed to determine total H<sub>2</sub>O<sub>2</sub> levels in solution. The values with MgCl<sub>2</sub> were considered as 100%. One way ANOVA and a posthoc Tukey with  $p < 0.05$  was performed. **(c)** MAPK activation. *Phaseolus* leaves were infiltrated *in planta* with 40  $\mu$ M FB1,  $1 \times 10^8$  CFU/ml Pst, 40  $\mu$ M sphinganine (SN) or 1 mM salicylic acid (SA); then, at the indicated times, leaf sections were cut and soluble protein fractions were obtained to determine in-gel MBP phosphorylation to estimate MAPK activity. Complete time courses and infiltration with MgCl<sub>2</sub> or Silwet L-77 as controls were performed and are shown in Supplemental Fig. S2. Experiments are representative of at least three biological replicates.

in necrosis processes. As a control, infiltration of MgCl<sub>2</sub> developed only a light circle caused by the slight wound (Fig. 1a, right side in both leaves). In order to corroborate that the FB1 and Pst treatments were inducing cell death, solute leakage was measured. Figure 1b shows that both, toxin and pathogen induced electrolyte release, but the kinetics and extent were faster and higher, respectively, with the Pst treatment as compared to the one elicited by the toxin.

**Elevation of LCBs.** FB1 elicits PCD and defense reactions through the elevation of LCBs as second messengers<sup>11,16</sup>. However, elevation of some sphingolipid species could not be detected in other non-host case<sup>8</sup>. Since in our system FB1 could be inducing a PCD related to an increase in endogenous LCBs, we measured LCB levels in the FB1- and Pst-infiltrated leaves. Figure 2a shows the determination of endogenous phytosphingosine, a LCB, upon FB1 or Pst infiltration. We observed phytosphingosine increases of 1.5 to 3-fold along the infiltration time course with either treatment. Although the kinetics and maximal extent of the LCB elevation were not identical for FB1 and Pst, there were coincident times of phytosphingosine rise (0.5 and 24h), showing a 2- to 3-fold

increase over the LCB levels measured in control leaves. These results indicated that both treatments induced LCB elevation in *Phaseolus* leaves.

**H<sub>2</sub>O<sub>2</sub> generation.** Another known response in plant immunity is the early generation of H<sub>2</sub>O<sub>2</sub><sup>17,35,36</sup>. For this reason, we measured this reactive oxygen species with a soluble assay in both PCD inducing treatments (Fig. 2b). The results showed that FB1 and Pst treatments induced an apparent significant generation of H<sub>2</sub>O<sub>2</sub> at 8 h upon FB1 infiltration and at 4 and 8 h upon Pst infiltration. However, statistical significance was not supported by tests (see Fig. legend).

**MAPK activation.** MAPK activation has been demonstrated to be downstream LCB surge in Arabidopsis PCD<sup>11</sup>. In order to get further support to the idea that the two treatments (FB1 and Pst) that induced PCD-HR were fully comparable in terms of the LCB elicitation, we investigated the possible activation of MAPKs upon FB1 and Pst infiltration of *P. vulgaris* leaves (Fig. 2c). In addition, we tested MAPK activation upon infiltration of SN, a LCB that elicits PCD-HR and that is precursor of phytosphingosine<sup>11</sup>. We detected the activation of a 48 kDa MAPK with the three treatments (Fig. 2c). The MAPK nature of the phosphorylation was corroborated by the specificity of the phosphorylated substrate i.e., myelin basic protein but not of histone or casein (Supplementary Fig. S1a,b) and the recognition of the 48 kDa band by antibodies directed against two typical MAPK, ERK1 and ERK2, and to their phosphorylated forms (Supplementary Fig. S1c). MgCl<sub>2</sub> infiltration showed an activation of the same MAPK at 5 and 10 min that probably involved the slight wound effect due to the infiltration procedure (Supplementary Fig. S2a). While FB1 and SN showed a MAPK activation at 45 and 240 min, Pst displayed a sustained activation as long as 480 min after infiltration (Fig. 2c, Supplementary Fig. S2a–d). The molecular mass of the detected MAPK was similar to the AtMPK6 from *Arabidopsis thaliana* and to the NtSIPK from *Nicotiana tabacum*<sup>37,38</sup>. The band, strongly phosphorylated in the presence of FB1, Pst and exogenous SN was dramatically labeled upon SA treatment (Fig. 2c, Supplementary Fig. S2a–e), a recognized mediator in plant immunity and an orthologue of MPK6 in Arabidopsis<sup>37,38</sup>. These results indicated that a MAPK commonly associated with defense responses was activated in conditions in which an elevation of an endogenous LCB occurs upon *Phaseolus* exposure to Pst.

**H<sub>2</sub>O<sub>2</sub> accumulation at the lesion.** We explored whether FB1 and Pst promoted *in situ* H<sub>2</sub>O<sub>2</sub> accumulation in the infiltrated tissue by using DAB staining (Fig. 3). The lesion induced by either FB1 or Pst was clearly visible at 24 h in the case of Pst and at 48 h in the case of FB1 (Fig. 3a). After direct infiltration, *in situ* H<sub>2</sub>O<sub>2</sub> formation was detected upon MgCl<sub>2</sub>, FB1 or Pst immediately after inoculation (0 h) (Fig. 3b). Between 18 and 24 h after infiltration, we detected H<sub>2</sub>O<sub>2</sub> accumulation in both treatments. The brown precipitate progressively augmented at 48 h. These results confirmed that both FB1 and Pst shared as a common feature the H<sub>2</sub>O<sub>2</sub> accumulation. No H<sub>2</sub>O<sub>2</sub> stain was observed in the control treatment.

**Accumulation of H<sub>2</sub>O<sub>2</sub> in the chloroplast is induced by treatments with FB1 or Pst.** We examined the DAB stained tissues under the microscope in order to establish the location of the precipitate accumulation. In both experimental treatments, H<sub>2</sub>O<sub>2</sub> accumulated in the chloroplast (Fig. 3c, central and right panels) but it was absent in the control leaves (Fig. 3c, left panel). This suggests that the possible origin of the accumulated H<sub>2</sub>O<sub>2</sub> in FB1 and Pst treatments is the chloroplast.

**Chloroplast fluorescence is compromised upon FB1 or Pst treatments.** H<sub>2</sub>O<sub>2</sub> could be formed in the chloroplast as a result of impairment of the photosynthetic function. Our first approach to explore the functional status of the chloroplast treated with FB1 or Pst was to examine chloroplast structure using its autofluorescence by confocal microscopy (Fig. 4). Figure 4a shows images recorded at 8, 18 and 24 h after MgCl<sub>2</sub>, FB1 or Pst treatments. As it can be observed, chloroplasts from *Phaseolus* leaves that were MgCl<sub>2</sub>-infiltrated showed similar morphology, distribution and emission of chlorophyll fluorescence throughout this time course. The FB1 treated plants (Fig. 4a) showed an apparent decrease in the chlorophyll fluorescence signal at 24 h, but the graph in Fig. 4b shows that dispersion of data gave no significant difference between the control and FB1 fluorescence intensity values at 24 h. In contrast, Pst-treated plants (Fig. 4a, right column) showed a clear decrease of the fluorescence emission at 18 h (Fig. 4b). This decrease was more evident at 24 h when the signal was very low. These results can be explained by impairment of the photosynthetic activity of the treated leaves. To analyze this hypothesis further, the fluorescence emitting area and the fluorescence intensity per pixel were measured. While the first parameter correlates with the number of functional chloroplasts (Fig. 4b), the latter is an indication of the chloroplast fitness to perform photosynthetic activity per area unit (pixel) (Fig. 4c). Both parameters were unchanged in the chloroplasts from control plants. In the case of FB1-treated plants, a significant decay in the fluorescence emitting area was observed after 24 h (30% lower than in MgCl<sub>2</sub>-treated plants) (Fig. 4b). In Pst-treated plants, a clear decay in the fluorescence emitting area was observed at 18 h (64% lower as compared to the MgCl<sub>2</sub>-treated plants), with no significant decrease at 24 h (70% lower than MgCl<sub>2</sub>-treated plants) (Fig. 4b). However, neither FB1- or Pst-treated plants showed a significant decay in the fluorescence intensity per pixel as compared to the control (Fig. 4c). Thus, in the case where the photosynthetic activity was compromised, it could primarily be associated to a decrease in the number of functional chloroplasts with FB1 and or Pst, rather than with an overall decay in the activity of each chloroplast.

**Early and similar impairments of the photosynthetic activity are caused by FB1 and Pst treatments.** While autofluorescence measurements were a good indicator of photosynthetic impairment, we explored the effect of FB1 and Pst on the photosystem II (PSII) activity. Thus, we measured the chl *a* fluorescence induction curve (OJIP curve) between 0 h (pre-infiltration sampling) and 48 h (0, 8, 18, 24 and 48 h). Figure 5a–c shows the average curves of fluorescence emission. No significant changes in the control leaves (MgCl<sub>2</sub>-infiltrated, Fig. 5a)

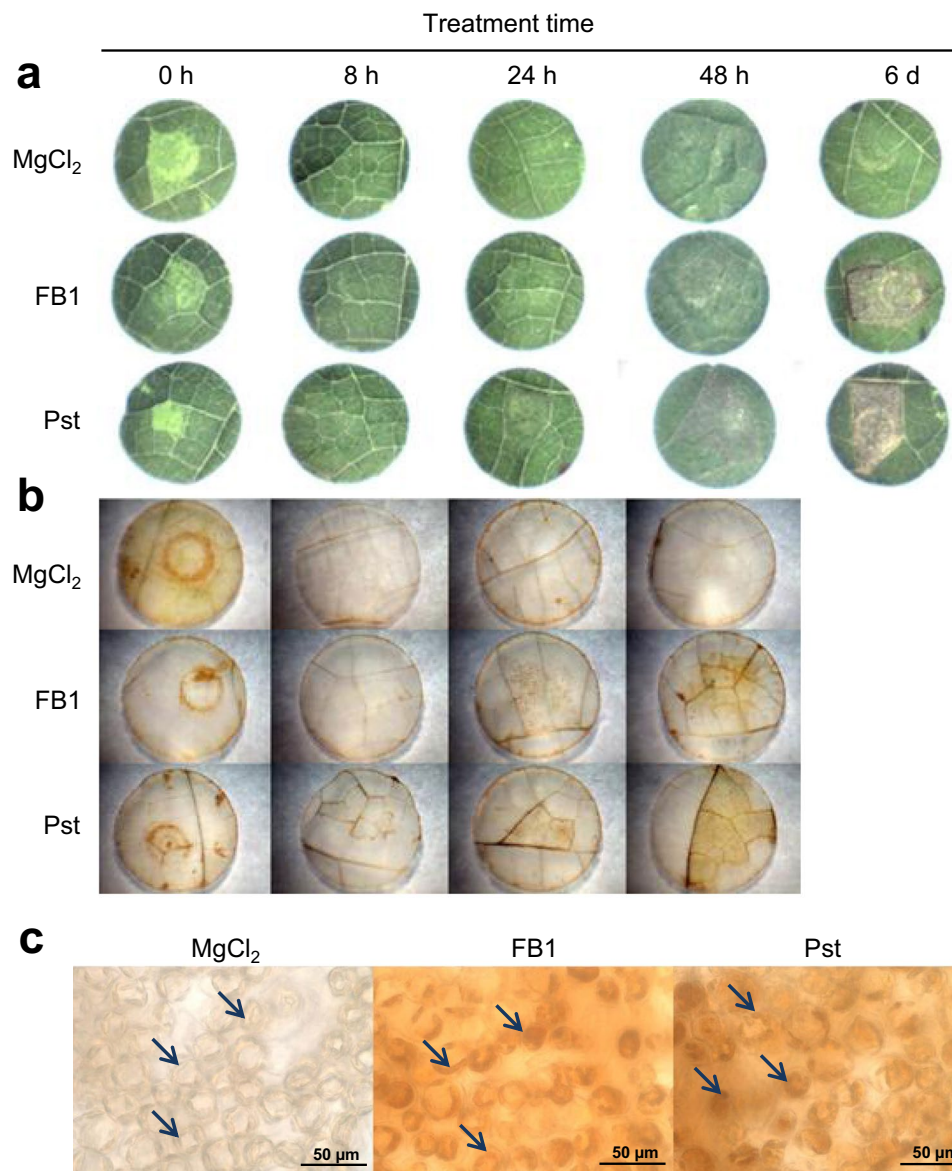


**Figure 3.** The PCD-HR lesions produced by FB1 and Pst treatments contain chloroplasts with H<sub>2</sub>O<sub>2</sub> inside. (a) Time progression of the PCD-HR lesion. Leaves were infiltrated *in planta* with 10 mM of MgCl<sub>2</sub>, 10 μM of FB1 or  $1 \times 10^8$  of CFU/ml of Pst, then leaf disks with the infiltrated regions were cut and pictures taken at the indicated times. (b) *In situ* generated H<sub>2</sub>O<sub>2</sub>. Experiment was as in A, but leaf disks were subjected to the DAB reaction. (c) Magnification of the tissue with positive DAB reaction. Labeling of chloroplasts with the brown-reddish precipitate containing H<sub>2</sub>O<sub>2</sub> is indicated by the arrows. The experiments shown are representative of four biological replicates.

were found as indicated by the low scattering of the curves, especially in phases O-I, at all infiltration times under study. This implied that the MgCl<sub>2</sub> infiltration produced only slight perturbations in the photosynthetic activity at the time span of 48 h. However, Fig. 5b,c clearly showed, respectively, that the FB1 and Pst infiltration produced impairments in the photosynthetic activity as a function of the treatment time.

We compared the change in the fluorescence intensity at O, L, K, J, I and P steps as a function of the time of exposure to MgCl<sub>2</sub> (Fig. 5d), FB1 (Fig. 5e) or Pst (Fig. 5f). Figure 4e shows that the earliest apparent decrease on chl *a* fluorescence occurred at 12 h with FB1 and at 8 h with Pst. In the case of prompt chlorophyll fluorescence, the first statistically significant decrease took place at 24 h for FB1-treated plants while with Pst treatment it occurred after 12 h (Fig. 5f). JI and IP phases presented the major changes in both treatments at 24 and 48 h but were more pronounced with Pst. Statistical significance was performed for all curves by multivariate hierarchical clustering analysis (Fig. 5g-i). The decrease in the early decay of the J step with Pst can be interpreted as a decrease in the capacity to perform QA reduction (photochemical phase of PSII), meanwhile the decrease in the JI and IP phases could reflect loss of electron transfer between PSII to Photosystem I (PSI). Therefore, the most affected part of the photosynthetic process that was associated to LCB surges was the electron transport.

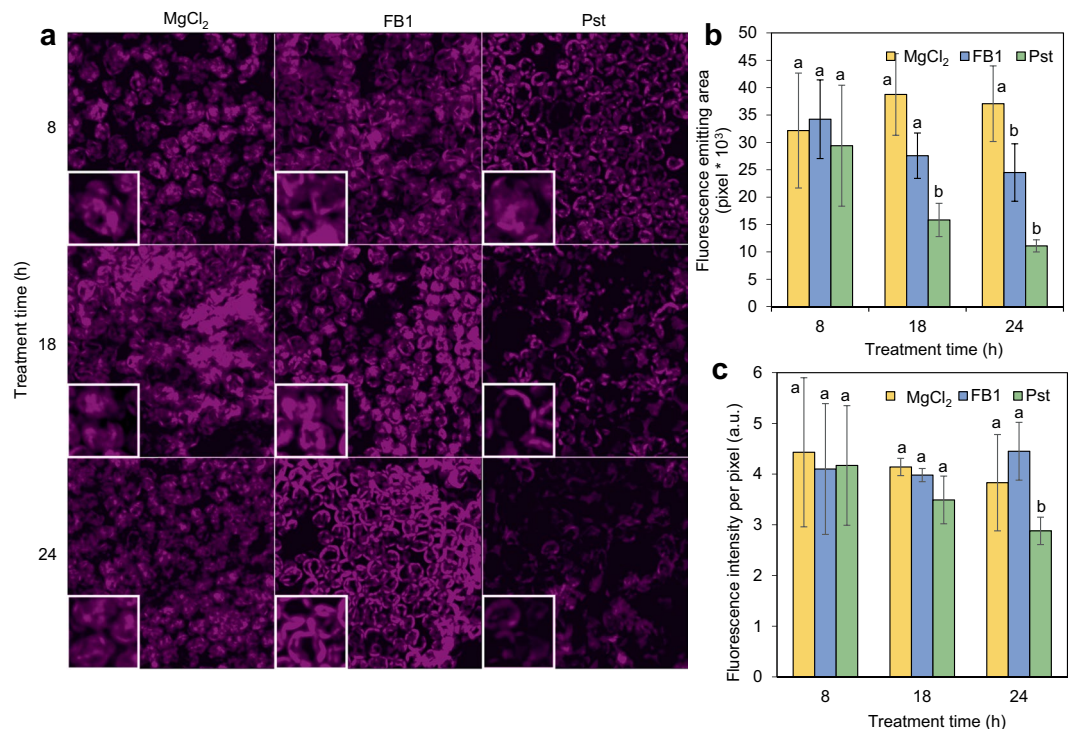


**Figure 4.** FB1 and Pst produce a loss of chlorophyll fluorescence. (a) Chloroplast fluorescence. *Phaseolus* leaves were infiltrated *in planta* with 10 mM MgCl<sub>2</sub>, 10 μM FB1 or 1 × 10<sup>8</sup> CFU/ml Pst. At the indicated times, sections of the infiltrated tissue were analyzed by confocal microscopy. Fluorescent signal is shown in magenta color. (b) Average value of the fluorescence emission area. (c) Average value of the fluorescence intensity per pixel. The images shown are representative of three biological replicates.

In order to know the state of the energy flow parameters, OJIP curves were analyzed by using the JIP-test model<sup>39,40</sup>. These parameters are presented in the form of radar plots (Fig. 6) and were calculated using the average curves in Fig. 5a–c. The comparison of data from leaves treated with FB1 or Pst for every time, i.e. 8 h, 18 h, 24 h and 48 h (Fig. 6) revealed a striking similarity in the magnitude and pattern of effects on JIP-test parameters. In the leaves exposed to FB1 and Pst for 18 h (Fig. 6), the total performance photosynthetic index (PI<sub>tot</sub>) parameter was the most negatively affected. According to the PI<sub>tot</sub> calculation, the decrease was mainly due to a decrease in the absorption per reaction center component (ABS/RC), i.e. an alteration of the ratio of the absorbed energy and the number of functional reaction centers. Therefore, there was a decrease in the number of functional PSII units. This result was in agreement with the information given by the images of confocal microscopy (Fig. 4a,b). In addition, the values of the yield of energy dissipation per reaction center (DI/ABS and DI/RC, respectively), dramatically enlarged upon 18 h of FB1 or Pst exposure.

Another photosynthetic parameter negatively affected after 18 h of exposure to FB1 or Pst was the electron carrier pool per reaction center (EC/RC). Such result was expected as the JI and IP phases were the most impaired. Based on the JIP algorithm analysis, increases in LCB were due to either the loss in the total pool of electron carriers or to the compromised turnover capacity of PSII, reducing the carrier molecules.

Together, these results suggest that both experimental treatments decreased the number of functional PSII reaction centers and the electron carriers.

**Disconnection between PSII and PSI is promoted by FB1 or Pst treatments.** The OJIP-test suggested that one of the major impairments of photosynthesis during PCD elicited by LCBs was the flow of electron carriers per active reaction center. This can be directly determined by measuring the linear electron flow between PSII and PSI by reflectance changes at 820 nm. Modulated light reflection (MR) is an approach to assess the oxidation state of P700<sup>+</sup> and PC<sup>+</sup><sup>41–43</sup>. MR was measured in parallel to the chl *a* fluorescence at pre-infiltration (0 h) and 10, 24 and 30 h after MgCl<sub>2</sub>, FB1 or Pst treatment (Fig. 7). MR experimental curves were normalized to the values at 0 h (pre-infiltration) for each condition to simplify the comparison.

MR determinations of leaves infiltrated with MgCl<sub>2</sub> and with 0 h exposure to FB1 (Fig. 7a) or to Pst (Fig. 7b) leaves showed that plants behaved in similar manner. The first phase, a fast phase (MR<sub>fast</sub>), occurring in approximately a time span of 0.001 and 0.01 s, reflects the levels of P700<sup>+</sup> and PC<sup>+</sup> (the oxidized forms). The second phase, a slow phase (MR<sub>slow</sub>) resolved in a span of 0.01 to 0.1 s, showed the progressive reduction of P700<sup>+</sup> and of PC due to the electrons coming from PSII, thus illustrating the connectivity of the electron transport between the two photosystems. Hence, this signal correlates with the PSII functionality and the activity of the electron transport chain between the two photosystems.

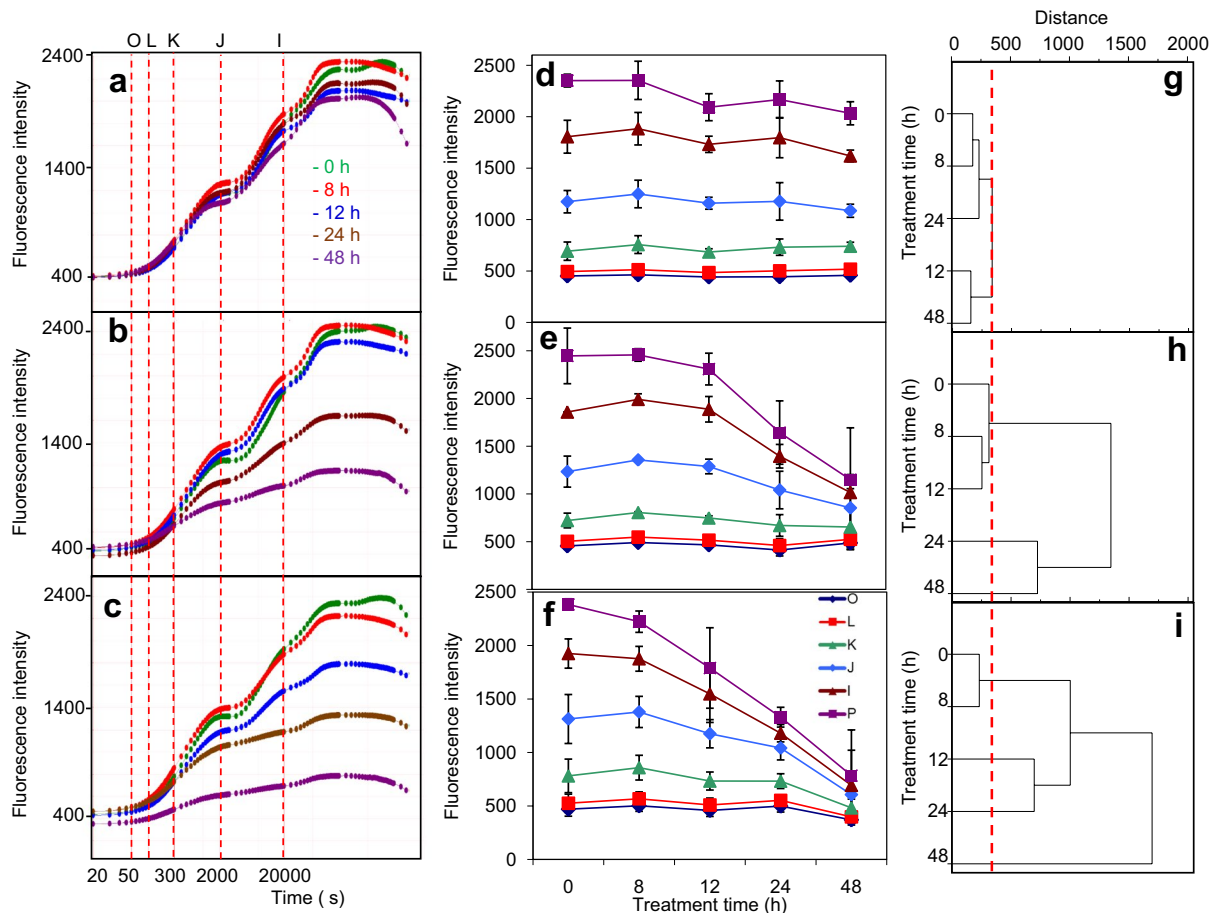


**Figure 5.** FB1 and Pst produce a decrease of chlorophyll *a* fluorescence upon treatments with FB1 or Pst. Chlorophyll *a* fluorescence was measured *in planta* in the infiltrated zones of the leaves. Panels a–c show the average OJIP transients for leaves infiltrated with (a) 10 mM MgCl<sub>2</sub>, (b) 10 μM FB1 or (c) 1 × 10<sup>8</sup> CFU/ml Pst at the indicated times. Panels (d–f) show the average value of each fluorescent step (OLKJIP) of leaves infiltrated with (d) 10 mM MgCl<sub>2</sub>, (e) 10 μM FB1 or (f) 1 × 10<sup>8</sup> CFU/ml Pst, respectively, at the indicated times. Curves and values represent the average ± SD of four biological replicates. Step O was measured at 50 μs, L at 150 μs, K at 300 μs, J at 2000 μs, I at 30,000 μs and P when fluorescence reached its maximum. (g–i) Statistical differences for each time point were estimated by multivariate hierarchical clustering analysis for MgCl<sub>2</sub> (g), FB1 (h) and Pst (i). Values of the O, L, K, J, I and P were used to estimate the Euclidian distance and were clustered by group average. The longer the distance in a cluster, the more different two time points were. To estimate the threshold of significance, the maximum distance in MgCl<sub>2</sub> data set was used as reference. Red dotted line describes the threshold for significance, in such case a node situated at the left of the red line is considered not significant. OJIP plots were constructed from data acquired with the HandyPEA instrument as described under Materials and methods section and processed by the Biolyzer 3.0 software, Bioenergetics Laboratory, Geneva, Switzerland.

Determination of MR in FB1-treated plants is shown in Fig. 7a. The fast initial phase of the MR signal was characterized by a decrease of the MR values in the span from 300 μs to 30 ms, when P700<sup>+</sup> and PC<sup>+</sup> presented maximum accumulation. This was followed by a slow (400–500 ms) positive phase caused by the gradual reduction of P700<sup>+</sup>. However, the curves of the leaves treated with FB1 for 24 and 30 h showed a 40% decrease of the MR<sub>fast</sub> phase compared to the 0 h curve, indicating that the total accumulation of PC<sup>+</sup> and P700<sup>+</sup> was affected by the FB1 treatment. Additionally, the MR<sub>slow</sub> was significantly affected at 30 h by the FB1 treatment. This could be explained by a loss in the efficiency of the electron transport chain to re-reduce the pool of P700 or/and PC upon the actinic illumination. However, plants treated with FB1 after 24 h showed a maximum value of the MR recovery after the fast phase, indicating that the electron transport between PSII and PSI units was still functional but was lost later after 30 h of FB1 exposure.

In the case of the pathogen treatment, the Pst control (0 h) displayed a similar curve to the FB1 control (Fig. 7b). MR<sub>slow</sub> phase at 10 and 24 h showed a decrease in total amplitude of 40% and 50%, respectively, when compared to the 0 h curve. Contrary to the FB1 curve at 24 h, the Pst curve showed that the re-reduction of P700 after 0.03 s almost completely disappeared. This meant that the electron transport between the two photosystems was impaired, indicating loss of the electron transport capacity between PSII and PSI.



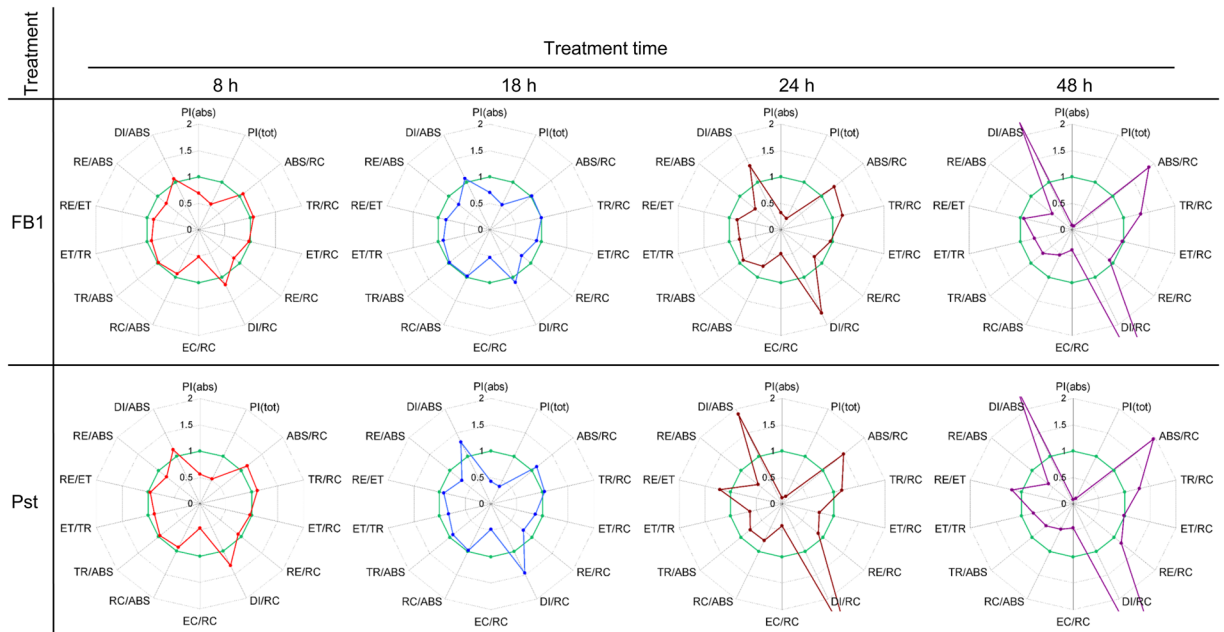


**Figure 6.** FB1 and Pst alter the same OJIP-test parameters. Average OJIP curves shown in Fig. 5 were used to calculate OJIP-test parameters. All parameters were normalized to the control value (pre-infiltrated plants) and represented in the radar plots shown. PI(abs) refers to photosynthetic performance index on absorption bases. PI(tot) refers to total photosynthetic performance index. ABS/RC refers to absorption per active PSII reaction center. TR/RC refers to trapping probability per active PSII reaction center. ET/RC refers to the probability of electron transport beyond  $Q_A$  per active PSII reaction center. RE/RC refers to the probability of an electron to be used in the reduction of final acceptors per active PSII reaction center. DI/RC refers to proportional energy dissipated by heat or fluorescence per active PSII reaction center. EC/RC refers to the rate of turnover by electron carriers per active PSII reaction center (which is estimated as the complementary area over the OJIP curve). RC/ABS is reciprocal of ABS/RC (see above). TR/ABS refers to the quantum yield for primary photochemistry. ET/TR refers to the yield for electron transport. RE/ET refers to the probability of an electron traveling through the electron transport chain to be used in the reduction of end acceptors. RE/ABS refers to the total quantum yield of photosynthesis. DI/ABS refers to quantum yield for energy dissipation. Note that OJIP-test parameters were calculated from average OJIP curves in Fig. 5, hence the statistical significance of these parameters is based on Fig. 5g–i. The OJIP parameters shown in the eight radar plots were obtained from the data in Fig. 5 using the Biolyzer 3.0 software, Bioenergetics Laboratory, Geneva, Switzerland.

### Chloroplast integrity and ultrastructure are compromised upon FB1 and Pst treatments.

Changes in photosynthetic functionality is associated with changes in grana stacking<sup>44</sup>. This is manifested by alteration of the efficiency of the electron transport between PSII to PSI<sup>45</sup>, the collapse of the proton gradient<sup>46</sup>, and the impairment of the lateral heterogeneity of the thylakoid membrane components<sup>47</sup>. In order to explore this possibility, the details of the chloroplast structure were investigated by transmission electron microscopy (Fig. 8b,c Supplementary Fig. S3). The control samples showed typical elongated chloroplasts with intact and well stacked thylakoid membranes and very well defined outer and thylakoid membranes (Fig. 8a). In contrast, chloroplasts from the FB1- and Pst-treated leaves (Fig. 8b,c; Supplementary Fig. S3) showed a rounded shape, very highly unstructured grana and thylakoid membranes at different states of disintegration, suggesting that a progressive process of chloroplast destruction was taking place. It was clear that FB1 and Pst treatment induced alterations of the electron transport capacity of PSII that were already detectable at 8 h (Fig. 6) and progressed until a visible macroscopic phenotypical alteration appear.

We calculated the so-called L-band from the average OJIP curves in Fig. 5a–c, as an additional way to confirm that the photosynthetic impairment was caused by alterations in thylakoid ultrastructure. In case of alteration in PSII unit connectivity, a positive band between 20  $\mu$ s and 300  $\mu$ s (L-band)<sup>48–50</sup> should appear in the OJIP transient. Figure 8d,e shows relative changes in fluorescence between 20  $\mu$ s and 300  $\mu$ s ( $\Delta W_{OK}$ ), where the L-band occurs. In both figures, it was possible to observe a clear positive band at 24 h for FB1 and 18 h for Pst. This confirms the observed disconnection between PSI and PSII (Fig. 6). Altogether, MR, TEM and L-band analysis confirmed that impairment of photosynthetic activity induced by FB1 and Pst led to disruption of thylakoid organization.

### Discussion

In this work, we have studied how two independent treatments that induce PCD elicited by LCBs have the same effect over the function and structure of the chloroplast. Given the role of this organelle on cell function, these results suggest that the chloroplast decay during PCD is an effective and irreversible mechanism that leads to cell death as a defense strategy against non-host pathogens. In detail, we show that the photosynthetic failure

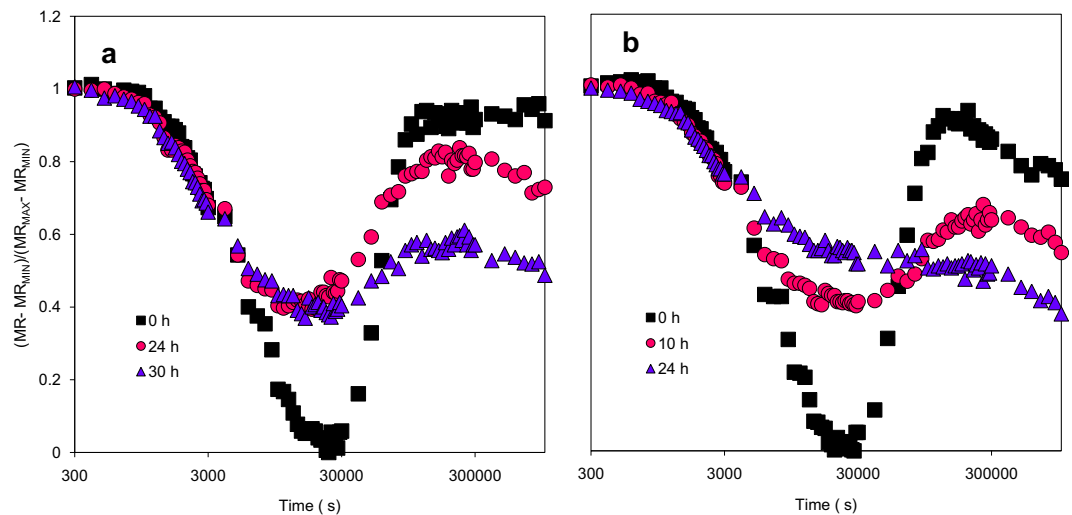


**Figure 7.** FB1 and Pst affect connectivity between PSII and PSI in leaves infiltrated with FB1 or Pst. Modulated reflection (MR) of 820 nm light was measured *in planta* to determine the redox state of P700 in the infiltrated regions of the plants. MR kinetics from leaves infiltrated with (a) 10  $\mu$ M FB1 or (b)  $1 \times 10^8$  CFU/ml Pst at the indicated times. Values were normalized to the pre-infiltration values. MR signal was collected in parallel to the OJIP transients (Fig. 5) by exciting the sample with 3000  $\mu$ mol of photons/m<sup>2</sup>/s. Curves are representative of three biological replicates.

is preceded by LCB increase and MAPK activation and involves ROS formation. This indicates that the loss of functionality of the chloroplast is part of the mechanism by which PCD occurs and is one event in the non-host immunity manifested in the HR.

In order to demonstrate the relation between all these events, the experimental framework consisted of a comparison of Pst and FB1 effects on chloroplast function in *Phaseolus vulgaris*. Pst (*Pseudomonas syringae* pv. *tomato*) is a bacterial non-host pathogen for *Phaseolus vulgaris*, while FB1 is an inducer of LCB elevation that leads to PCD<sup>11,16,24</sup>. FB1 has proven to lead to the manifestation of an HR and defense reactions against pathogens<sup>11,16,35</sup>. The comparison between these treatments revealed striking similarities that included same biochemical features (LCB rise, MAPK activation and H<sub>2</sub>O<sub>2</sub> production), structural changes in the chloroplast (thylakoid unstacking and deformation of the chloroplast) and photosynthetic function impairment. The experimental comparison of both treatments allowed the identification of several pieces of the mechanism underlying plant defense under a scheme of PCD.

In *Arabidopsis*, FB1 induced an HR-like wound due to a LCB accumulation acting as second messengers<sup>11,16,35</sup>. Here, we also show that FB1 in *Phaseolus vulgaris* induces a LCB rise and downstream events of HR such as MPK activation and ROS production. The parallelism found here for Pst, a non-host pathogen, shows that LCBs are also involved in this type of immune response. Although, during the non-host immunity response observed in *Nicotiana benthamiana* with *Pseudomonas cichorii*, an increase in gene transcription of SPT subunits was essential to produce HR, LCB changes were undetectable<sup>8</sup>. The successful LCB detection in our case of non-host defense could be due to a difference in LCB extraction and/or to the frequent sampling during the intermittent and irregular LCB increase pattern that contrasts with regular LCB rises induced by pathogens in the PAMPs-triggered immunity (PTI) and in the Effector-triggered immunity (ETI) schemes<sup>51</sup>. Therefore, the LCB surge seems to follow a profile that is specific to the type of immunity. In the case of the PTI, the rise of LCB occurs as a unique, early and short-life peak upon exposure to the pathogen while in the ETI occurs as a sustained and high LCB surge<sup>51</sup>. It can be suggested that non-host immunity, that contains PTI and ETI features, shows a LCB surge profile that takes elements from both PTI and ETI, which are associated with this non-host HR.

MAP cascades are activated upon exposure to several stresses. Based on the specificity of substrate phosphorylation and antibody reactivity, the present work shows that a MAPK is activated in *Phaseolus* leaves upon FB1, SN and Pst exposure. This result indicates that endogenous and exogenous LCBs are able of eliciting the same response, i.e. the same MAPK activation. In the case of responses to pathogen attack, the most common MAPKs activated are MPK3 and MPK6<sup>37,52</sup>. In addition, the latter has been shown to be the one activated downstream LCB accumulation<sup>11</sup>. Therefore, the molecular mass, the activation by LCB and by SA, and the analogous time response pattern to *Pseudomonas syringae* pv. *tomato* strongly indicate that the MAPK activated is MPK6 as it occurs in other systems<sup>11</sup>. However, immunoprecipitation with specific antibodies directed against the *Phaseolus* enzyme must settle this point.

It is possible that very low levels of H<sub>2</sub>O<sub>2</sub> generated at early times and undetected by DAB stain, initiate PCD as part of the initial signaling events that include LCB surge and MAPK activation. Such ROS generation that we were unable to detect has been described as an initial H<sub>2</sub>O<sub>2</sub> burst in defense against pathogens, but takes place outside the chloroplast<sup>11,16,36</sup>.

After the signaling steps: LCB increases and MAPK activation, the chloroplast starts a program to stop photosynthesis. The pattern of decay of photosynthesis upon LCBs accumulation was very similar between the FB1

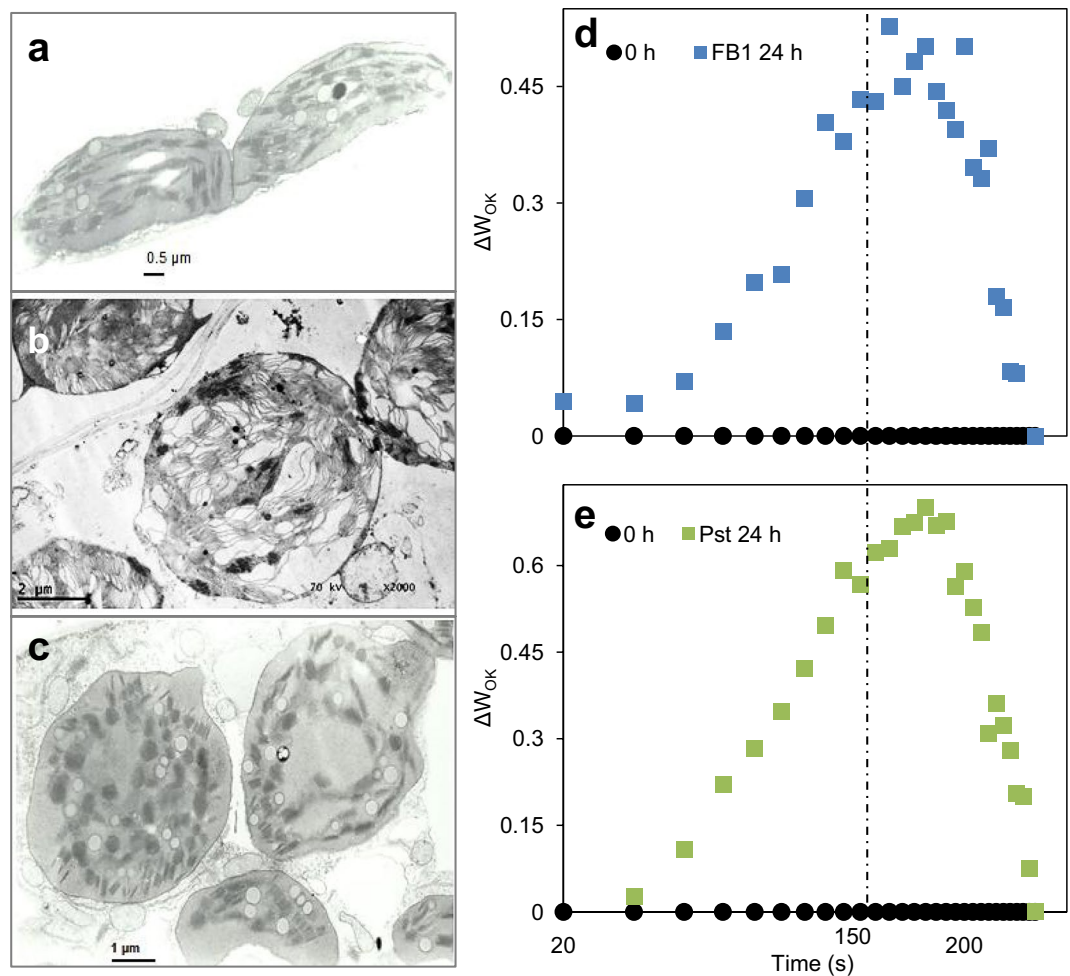


**Figure 8.** FB1 and Pst induce unstacking and brakeage of thylakoid membranes. Representative transmission electron microscopy images from chloroplasts from leaves after 24 h of *in planta* infiltration with (a) 10 mM MgCl<sub>2</sub>, (b) 10 μM FB1 or (c) 1 × 10<sup>8</sup> CFU/ml Pst. Chlorophyll *a* fluorescence L-band (150 μs) (ΔW<sub>OLK</sub>) from leaves infiltrated with (d) 10 μM FB1 and (e) 1 × 10<sup>8</sup> CFU/ml Pst. L-Band was obtained by normalizing the fluorescence intensity between O (20 μs) and K (300 μs) steps of the average OLKJIP transient obtained in Fig. 5. Control or 0 h infiltration sample (squares) and 24 h infiltrated sample (triangles) are shown. Curves are representative of three biological replicates.

and Pst treatments. Three main characteristics were observed: (1) a decrease in the number of functional reaction centers of PSII; (2) the compromised ability of PSII to reduce the PQ and to sustain the electron transport towards PSI; (3) a loss in the PSII centers connectivity due to severe thylakoid unstacking. These shared features between the FB1 and Pst treatments make us hypothesize that the loss of function of the chloroplast is a well-organized process that has in common LCB surges and MAPK activation.

It is known that during pathogen infections the photosynthetic activity is interrupted<sup>20–22</sup>. The observed effect in this work over linear electron transport and its carriers (as shown by JIP-test and MR) indicates a size decrease of the pool of acceptors. This would lead to an increased amount of ROS accumulation in the chloroplast<sup>53,54</sup>. It is commonly accepted that ROS can be generated in the chloroplast via light sensitization<sup>55–57</sup> and this could be aggravated by an increase in excitation pressure. This explains why at 24 h, DAB stain detected high levels of H<sub>2</sub>O<sub>2</sub>, which occurred after the first major signs of photosynthesis inactivation started to appear.

Interestingly, it has been reported that PCD induced by FB1 requires light and it has been proposed that ROS produced in the chloroplast could be the second messengers that up-regulate SA synthesis by enhancing PAL activity leading to a PCD HR-like<sup>58</sup>. Also, based only on chloroplast ultrastructure, studies in *Arabidopsis*, one using FB1<sup>11</sup> and the other using *Pseudomonas syringae maculicola* 4326 avrRpt2<sup>58,59</sup> proposed that ROS formed in the organelle may cause disassembly of the photosystems. Altogether, the detected accumulation of H<sub>2</sub>O<sub>2</sub> in this work must have caused a destructive effect on the photosynthetic ensemble as revealed by the ultrastructural observations.

LCB accumulation produced by FB1 and Pst caused an eventual alteration of chloroplast morphology. It was in the rounded chloroplasts where the large peroxide accumulation occurred and in which thylakoids looked unstacked and broken. In support to this structural and functional damage, the so-called L-band was observed

in both FB1 and Pst treatments. The appearance of a positive L-band is attributed to failures in the connectivity between the photosystems<sup>48–50</sup>. For both treatments, the L-band was detected at the times when clear thylakoid unstacking was found. Therefore, the failure of connectivity is reasonably explained by the unstacking of the thylakoid membranes in the leaves exposed to the toxin or the pathogen.

Here we show that during PCD, just after the LCB accumulation and MAPK activation took place, a decrease in the chloroplast electron carriers occurred. This was followed by a large accumulation of ROS inside the chloroplast that lead to collapse the thylakoid membrane system. It is possible that ROS could catalyze the oxidation of the thylakoid membrane lipids. This is supported by the formation of H<sub>2</sub>O<sub>2</sub> inside the chloroplasts<sup>17</sup> and by the promotion of extensive chloroplast damage by FB1, that includes the degradation of proteins from the chloroplast stroma<sup>57</sup>. Degradation of core proteins from the photosynthetic complexes has been reported but in a model that involves a compatible plant-pathogen interaction<sup>59,60</sup>. In nature, several scavenging processes ensure a low concentration of ROS inside the chloroplast<sup>61</sup>. Therefore, an intermediary process is required to allow accumulation of ROS in the chloroplast; thus, a midway step between accumulation of LCBs and inactivation of the chloroplast would be required to shut down ROS scavenging processes. The decay of the photosynthetic machinery observed can be related to a silencing of the chloroplast protein expression<sup>62,63</sup> associated with an absence of the repair mechanism that produces the photodamage of PSII<sup>64–67</sup>. Therefore, the damaged photosystems would not be replaced by new ones<sup>68</sup> and the chloroplast would produce ROS via antenna sensitization due to excitation pressure<sup>69</sup>.

## Conclusions

We have shown that two agents inducing PCD by accumulation of LCBs led to the organized decay of the chloroplast function and structure. This is characterized by the decline of the light reactions of photosynthesis, which leads to the accumulation of ROS in the chloroplast. Thus, the observed HR-PCD involves signaling and executory steps that include the rise of LCBs, MAPK activation, collapse of both photosystems, massive ROS production and structural disintegration of the thylakoid membrane and the chloroplast. This orchestrated and programmed sequence of events leads the plant cell to its self-destruction as a defense strategy against dissemination of biotroph pathogens. The features of such molecular events may vary in other cases of PCD or in other forms of immunity but because of their impact on cell energetics, they seem to function as a stratagem to reach a point of no-return in the program of cell death in immunity.

Received: 19 September 2019; Accepted: 27 April 2020;

Published online: 25 June 2020

## References

1. Markham, J. E., Lynch, D. V., Napier, J. A., Dunn, T. M. & Cahoon, E. B. Plant sphingolipids: function follows form. *Curr. Opin. Plant Biol.* **16**, 1–8 (2013).
2. Berkey, R., Bendigeri, D. & Xiao, S. Sphingolipids and plant defense/disease: the “death” connection and beyond. *Front. Plant Sci.* **3**, 68, <https://doi.org/10.3389/fpls.2012.00068> (2012).
3. Magnin-Robert, D. *et al.* Modifications of sphingolipid content affect tolerance to hemibiotrophic and necrotrophic pathogens by modulating plant defense responses in *Arabidopsis*. *Plant Physiol.* **169**, 2255–2274 (2015).
4. Michaelson, L. V., Napier, J. A., Molino, D. & Faure, J.-D. Plant sphingolipids: Their importance in cellular organization and adaptation. *Biochim. Biophys. Acta* **1861**, 1329–1335 (2016).
5. Ng, C. K. Y., Carr, K., McAinsh, M., Powell, B. & Hetherington, A. M. Drought-induced guard cell signal transduction involves sphingosine-1-phosphate. *Nature* **410**, 596–599 (2001).
6. Coursol, S. *et al.* Sphingolipid signalling in *Arabidopsis* guard cells involves heterotrimeric G proteins. *Nature* **423**, 651–654 (2003).
7. Coursol, S. *et al.* *Arabidopsis* sphingosine kinase and the effects of phytosphingosine-1-phosphate on stomatal aperture. *Plant Physiol.* **137**, 724–737 (2005).
8. Takahashi, Y. *et al.* Serine palmitoyltransferase, the first enzyme in sphingolipid biosynthesis, is involved in non-host resistance. *Mol. Plant Microbe Interact.* **22**, 31–38 (2009).
9. Dutilleul, C. *et al.* Phytosphingosine-phosphate is a signal for AtMPK6 activation and *Arabidopsis* response to chilling. *New Phytol.* **194**, 181–191 (2012).
10. Lachaud, C. *et al.* Nuclear calcium controls the apoptotic-like cell death induced D-erythro -sphinganine in tobacco cells. *Cell Calcium* **47**, 92–100 (2010).
11. Saucedo-García, M. *et al.* MPK6, sphinganine and the *LCB2a* gene from serine palmitoyltransferase are required in the signaling pathway that mediates cell death induced by long chain bases in *Arabidopsis*. *New Phytol.* **191**, 943–957 (2011).
12. Peer, M., Bach, M., Mueller, M. J. & Waller, F. Free sphingobases induce RBOHD-dependent reactive oxygen species production in *Arabidopsis* leaves. *FEBS Lett.* **585**, 3006–3010 (2011).
13. Lam, E., Kato, N. & Lawton, M. Programmed cell death, mitochondria and the plant hypersensitive response. *Nature* **411**, 848–853 (2001).
14. Mur, L. A., Kenton, P., Lloyd, A. J., Ougham, H. & Prats, E. The hypersensitive response; the centenary is upon us but how much do we now? *J. Exp. Bot.* **59**, 501–520 (2008).
15. Keen, N. T., Ersek, T., Long, M., Bruegger, B. & Holliday, M. Inhibition of the hypersensitive reaction of soybean leaves to incompatible *Pseudomonas* spp. by blasticidin S, streptomycin or elevated temperature. *Physiol. Plant Pathol.* **18**, 325–337 (1981).
16. Shi, L. *et al.* Involvement of sphingoid bases in mediating reactive oxygen intermediate production and programmed cell death in *Arabidopsis*. *Cell Res.* **17**, 1030–1040 (2007).
17. Saucedo-García, M. *et al.* Reactive oxygen species as transducers of sphinganine-mediated cell death pathway. *Plant Signal. Behav.* **6**, 1616–1619 (2011).
18. Lachaud, C. *et al.* Dihydro sphingosine-induced programmed cell death in tobacco BY-2 cells is independent of H<sub>2</sub>O<sub>2</sub> production. *Mol. Plant* **4**, 310–318 (2011).
19. Liu, Y. *et al.* Chloroplast-generated reactive oxygen species are involved in hypersensitive response-like cell death mediated by a mitogen-activated protein kinase cascade. *Plant J.* **51**, 941–954 (2007).
20. Mühlentock, P. *et al.* Chloroplast signaling and lesion simulating disease 1 regulate crosstalk between light acclimation and immunity in *Arabidopsis*. *Plant Cell* **20**, 2339–2356 (2008).

21. Mur, L. A. *et al.* Accumulation of chlorophyll catabolites photosensitizes the hypersensitive response elicited by *Pseudomonas syringae* in *Arabidopsis*. *New Phytol.* **188**, 161–174 (2010).
22. Berger, S. *et al.* Visualization of dynamics of plant-pathogen interaction by novel combination of chlorophyll fluorescence imaging and statistical analysis: differential effects of virulent and avirulent strains of *P. syringae* and of oxylipins on *A. thaliana*. *J. Exp. Bot.* **58**, 797–806 (2007).
23. Lu, Y. & Yao, J. Chloroplasts at the crossroad of photosynthesis, pathogen infection and plant defense. *Int. J. Mol. Sci.* **19**, 3900, <https://doi.org/10.3390/ijms19123900> (2018).
24. Boccarda, M. *et al.* Early chloroplastic alterations analysed by optical coherence tomography during a harpin-induced hypersensitive response. *Plant J.* **50**, 338–346 (2007).
25. Abbas, H. K. *et al.* Fumonisin and AAL toxin induced disruption of sphingolipid metabolism with accumulation of free sphingoid bases. *Plant Physiol.* **106**, 1085–1093 (1994).
26. Yang, C.-H. *et al.* *hrp* Genes of *Erwinia chrysanthemi* 3937 are important virulence factors. *Mol. Plant-Microbe Interact.* **150**, 472–480 (2002).
27. Gutiérrez-Nájera, N. *et al.* Fumonisin B1, a sphingoid toxin, is a potent inhibitor of the plasma membrane H<sup>+</sup>-ATPase. *Planta* **221**, 589–596 (2005).
28. Thordal-Christensen, H., Zhang, Z., Wei, Y. & Collinge, D. Subcellular localization of H<sub>2</sub>O<sub>2</sub> in plants. H<sub>2</sub>O<sub>2</sub> accumulation in papillae and hypersensitive response during barley-powdery mildew interaction. *Plant J.* **11**, 1187–1194 (1997).
29. Gray, C., Collins, J. & Gebicki, J. M. Hydroperoxide assay with the ferric-xylenol orange complex. *Anal. Biochem.* **273**, 149–155 (1999).
30. Markham, J., Li, J., Cahoon, E. & Jaworski, J. Separation and identification of major plant sphingolipid classes from leaves. *J. Biol. Chem.* **281**, 22684–22694 (2006).
31. Cho, Y.-H. *et al.* Comparative study of naphthalene-2,3-dicarboxaldehyde and o-phthalaldehyde fluorogenic reagents for chromatographic detection of sphingoid bases. *Journal of Chromatography A* **977**(1), 69–76 (2002).
32. Schneider, C. A., Rasband, W. S. & Eliceiri, K. W. NIH Image to ImageJ: 25 years of image analysis. *Nat. Methods* **9**, 671–675 (2012).
33. Brandwagt, B. F., Kneppers, T. J. A., Van der Weerden, G. M., Nijkamp, H. J. & Hille, J. Most AAL toxin-sensitive *Nicotiana* species are resistant to the tomato fungal pathogen *Alternaria alternata* f. sp. *Lycopersici*. *Mol. Plant Microbe Interact.* **14**, 460–470 (2001).
34. Spassieva, S. D., Marham, J. E. & Hille, J. The plant disease resistance gene *Asc-1* prevents disruption of sphingolipid metabolism during AAL-toxin-induced programmed cell death. *Plant J.* **32**, 561–572 (2002).
35. Stone, J., Heard, J., Asai, T. & Ausubel, F. Stimulation of fungal mediated cell death by fumonisin B1 and selection of fumonisin B1-resistant (*fbr*) *Arabidopsis* mutants. *Plant Cell* **12**, 1811–1822 (2000).
36. Torres, M. A., Jones, J. D. G. & Dangl, J. L. Reactive oxygen species signaling in response to pathogens. *Plant Physiol.* **141**, 373–378 (2006).
37. Desikan, R., Clarke, A., Atherfold, P., Hancock, J. T. & Neill, S. J. Harpin induces mitogen-activated protein kinase activity during defence responses in *Arabidopsis thaliana* suspension cultures. *Planta* **210**, 97–103 (1999).
38. Zhang, S. & Klessig, D. Salicylic acid activates a 48-kDa MAP kinase in tobacco. *Plant Cell* **9**, 809–824 (1997).
39. Strasser, R. J., Srivastava, A. & Govindjee, G. Polyphasic chlorophyll *a* fluorescence transient in plants and cyanobacteria. *Photochem. Photobiol.* **61**, 32–42 (1995).
40. Strasser, R. J., Tsimilli-Michael, M. & Srivastava, A. Analysis of the chlorophyll fluorescence transient, in: G. C. Papageorgiou, Govindjee, (Eds.), *Chlorophyll a fluorescence: a signature of photosynthesis, Advances in Photosynthesis and Respiration*, Springer Dordrecht pp. 321–362 (2004).
41. Schansker, G., Srivastava, A., Govindjee, G. & Strasser, R. J. Characterization of the 820-nm transmission signal paralleling the chlorophyll *a* fluorescence rise (OJIP) in pea leaves. *Funct. Plant Biol.* **30**, 785–796 (2003).
42. Jiang, C. D. *et al.* Development of photosystems 2 and 1 during leaf growth in grapevine seedlings probed by chlorophyll *a* fluorescence transient and 820 nm transmission *in vivo*. *Photosynthetica* **44**, 454–463 (2006).
43. Strasser, R. J., Tsimilli-Michael, M., Qiang, S. & Goltsev, V. Simultaneous *in vivo* recording of prompt and delayed fluorescence and 820-nm reflection changes during drying and after rehydration of the resurrection plant *Haberlea rhodopensis*. *Biochim. Biophys. Acta* **1797**, 1313–1326 (2010).
44. Andersson, J. *et al.* Absence of the Lhcb1 and Lhcb2 proteins of the light-harvesting complex of photosystem II—effects on photosynthesis, grana stacking and fitness. *Plant J.* **35**, 350–361 (2003).
45. Barber, J. An explanation for the relationship between salt-induced thylakoid stacking and the chlorophyll fluorescence changes associated with changes in spillover of energy from photosystem II to photosystem I. *FEBS Lett.* **118**, 1–10 (1980).
46. Chow, W. S., Kim, E. H., Horton, P. & Anderson, J. M. Grana stacking of thylakoid membranes in higher plant chloroplasts: the physicochemical forces at work and the functional consequences that ensue. *Photochem. Photobiol. Sci.* **4**, 1081–1090 (2005).
47. Andersson, B. & Anderson, J. M. Lateral heterogeneity in the distribution of chlorophyll-protein complexes of the thylakoid membranes of spinach chloroplasts. *Biochim. Biophys. Acta* **593**, 427–440 (1980).
48. Strasser, R. J. The grouping model of plant photosynthesis: heterogeneity of photosynthetic units in thylakoids, in: G. Akoyunoglou, (Ed.), *Structure and molecular organization of the photosynthetic apparatus, photosynthesis: Proceedings of the 5th International Congress on Photosynthesis*. Halkidiki/Greece: Balaban International Science Services, Philadelphia, 727–737 (1981).
49. Strasser, R. J. & Greppin, H. Primary reactions of photochemistry in higher plants, in: G. Akoyunoglou, (Ed.), *Photosynthesis: Structure and Molecular Organisation of the Photosynthetic Apparatus*, Balaban International Science Services Philadelphia, USA, 717–726 (1981).
50. Strasser, R. J. & Stirbet, A. D. Heterogeneity of photosystem II probed by the numerically simulated chlorophyll *a* fluorescence rise (O–J–I–P). *Math Comput. Simul.* **48**, 3–9 (1998).
51. Peer, M., Stegmann, M., Mueller, M. J. & Waller, F. *Pseudomonas syringae* infection triggers *de novo* synthesis of phytosphingosine from sphinganine in *Arabidopsis thaliana*. *FEBS Lett.* **584**, 4053–4056 (2010).
52. Asai, T. *et al.* MAP kinase signaling cascade in *Arabidopsis* innate immunity. *Nature* **415**, 977–983 (2002).
53. Vass, I. Role of charge recombination processes in photodamage and photoprotection of the photosystem II complex. *Physiol. Plant* **142**, 6–16 (2011).
54. Vass, I. Molecular mechanisms of photodamage in the Photosystem II complex. *Biochim. Biophys. Acta* **1817**, 209–217 (2012).
55. Kim, C. *et al.* Chloroplasts of *Arabidopsis* are the source and a primary target of a plant-specific programmed cell death signaling pathway. *Plant Cell* **24**, 3026–3039 (2012).
56. Asada, K. Production and scavenging of reactive oxygen species in chloroplasts and their functions. *Plant Physiol.* **141**, 391–396 (2006).
57. Xing, F., Li, Z., Sun, A. & Xing, D. Reactive oxygen species promote chloroplast dysfunction and salicylic acid accumulation in fumonisin B1-induced cell death. *FEBS Lett.* **587**, 2164–2172 (2013).
58. Yao, N. & Greenberg, J. T. *Arabidopsis ACCELERATED CELL DEATH2* modulates programmed cell death. *Plant Cell* **18**, 397–411 (2006).
59. Jelenska, J. *et al.* A J-domain virulence effector of *Pseudomonas syringae* remodels host chloroplasts and suppresses defenses. *Curr. Biol.* **17**, 499–508 (2007).
60. Cheng, D.-D. *et al.* Photoinhibition and photoinhibition-like damage to the photosynthetic apparatus in tobacco leaves induced by *Pseudomonas syringae* pv. *tabaci* under light and dark conditions. *BMC Plant Biol.* **16**, 29 (2016).

61. Tyystjärvi, E. Photoinhibition of photosystem II and photodamage of the oxygen evolving manganese cluster. *Coord. Chem. Rev.* **252**, 361–376 (2008).
62. Zavafer, A., Cheah, M.H., Hillier, W., Chow, W.S. & Takahashi S. Photodamage to the oxygen evolving complex of photosystem II by visible light. *Sci. Rep.* <https://doi.org/10.1038/srep16363> (2015).
63. Zavafer, A., Koinuma, W., Chow, W.S., Cheah, M.H. & Mino, H. Mechanism of photodamage of the oxygen evolving Mn cluster of photosystem II by excessive light energy. *Sci. Rep.* <https://doi.org/10.1038/s41598-017-07671-1> (2017).
64. Nishiyama, Y. *et al.* Oxidative stress inhibits the repair of photodamage to the photosynthetic machinery. *EMBO J.* **20**, 5587–5594 (2001).
65. Nishiyama, Y., Allakhverdiev, S. I. & Murata, N. A new paradigm for the action of reactive oxygen species in the photoinhibition of photosystem II. *Biochim. Biophys. Acta* **1757**, 742–749 (2006).
66. Murata, N., Takahashi, S., Nishiyama, Y. & Allakhverdiev, S. I. Photoinhibition of photosystem II under environmental stress. *Biochim. Biophys. Acta* **1767**, 414–421 (2007).
67. Nishiyama, Y. & Murata, N. Revised scheme for the mechanism of photoinhibition and its application to enhance the abiotic stress tolerance of the photosynthetic machinery. *Appl. Microbiol. Biotechnol.* **98**, 8777–8796 (2014).
68. Osmond, C. B., Badger, M., Maxwell, K., Björkman, O. & Leegood, R. Too many photons: photorespiration, photoinhibition and photooxidation. *Trends Plant Sci.* **2**, 119–121 (1997).
69. Pospíšil, P. Molecular mechanisms of production and scavenging of reactive oxygen species by photosystem II. *Biochim. Biophys. Acta* **1817**, 218–231 (2012).

## Acknowledgements

This work was supported by the Dirección General de Asuntos del Personal Académico, Universidad Nacional Autónoma de México [PAPIIT-IN222815, IN220618]; Facultad de Química, Universidad Nacional Autónoma de México [PAIP 50009115]; and Consejo Nacional de Ciencia y Tecnología, México [238368]. The authors thank Dr. Reto Strasser for support along this work, Dr. Javier Plasencia for assessment with LCB determination, Dr. Rodolfo Paredes, Dr. Karina Jiménez-Durán and Dr. Ana Isabel Bieler-Antolin for transmission electron and confocal microscopy work, and Laura Carmona-Salazar, and Adelita Hernández González for technical help. The authors are profoundly grateful to Prof. Wah Soon Chow from the Australian National University for critical and English review of the manuscript.

## Author contributions

M.G.-R. and A.Z. designed the research, performed the experiments, analyzed the data and wrote the manuscript. A.G.-S., S.P.-B., M.S.-G., C.T.-A., S.V.-S. and B.K.-D. performed the experiments and analyzed data. All authors reviewed the manuscript.

## Competing interests

The authors declare no competing interests.

## Additional information

**Supplementary information** is available for this paper at <https://doi.org/10.1038/s41598-020-65186-8>.

**Correspondence** and requests for materials should be addressed to M.G.-R.

**Reprints and permissions information** is available at [www.nature.com/reprints](http://www.nature.com/reprints).

**Publisher's note** Springer Nature remains neutral with regard to jurisdictional claims in published maps and institutional affiliations.



**Open Access** This article is licensed under a Creative Commons Attribution 4.0 International License, which permits use, sharing, adaptation, distribution and reproduction in any medium or format, as long as you give appropriate credit to the original author(s) and the source, provide a link to the Creative Commons license, and indicate if changes were made. The images or other third party material in this article are included in the article's Creative Commons license, unless indicated otherwise in a credit line to the material. If material is not included in the article's Creative Commons license and your intended use is not permitted by statutory regulation or exceeds the permitted use, you will need to obtain permission directly from the copyright holder. To view a copy of this license, visit <http://creativecommons.org/licenses/by/4.0/>.

© The Author(s) 2020